International Journal of Nanoelectronics and Materials
IJNeaM
ISSN 1985-5761 | E-ISSN 2232-1535

Impact of Laser Annealing Duration on the Photodetectors of n-PSi/ZnO/Pt

Motahher A Qaeed

Department of Physical Sciences, Faculty of Science, University of Jeddah, Jeddah, Saudi Arabia
Corresponding author. Tel.: +9-665-039-10717; e-mail: maqayid@uj.edu.sa

ABSTRACT

This research was devoted to studying the effect of Nd:YAG laser pulses at different annealing times (30, 60, and 90 min) at a flux of 10 ns in air at room temperature on the performance of an n-PSi/ZnO-based metal-semiconductor-metal (MSM) UV detector. By coupling thermal and photon energy, heterojunctions of n-PSi/ZnO NCs were generated, highlighting a promising approach for developing renewable energy technologies through efficient light harvesting and conversion.In this work electro-photochemical etching were used at room temperature (27°C) to create n-type porous silicon (n-PSi) layers on Si (111) substrates. The substrates had an etched area of 1 cm^2 and measured 1.5 cm by 1.5 cm. The n-PSi thicknesses at various current densities (15, 30, and 45 mA/cm^2) were 9.6, 28.71, and 62.92 μm, respectively. To get rid of organic, oxide, and ionic impurities, standard RCA cleaning was used. A Teflon cell with a two-electrode configuration (Si anode, Pt cathode) and an electrolyte mixture of HF, ethanol, and H_2O_2 in a 2:1:1 volume ratio were utilized in the etching process. To create MSM photodetectors, samples were etched, then patterned with a photoresist and subjected to UV light. To change the n-PSi/ZnO NCs layer, post-fabrication annealing was carried out using an Nd:YAG laser (1064 nm, 350 mJ, 10 ns pulses) with a 10 cm focus lens at different durations (30, 60, 90 min), employing photon energy matching the Si bandgap. According to the study, annealing the n-PSi/ZnO NCs layer for 60 minutes at 700°C yielded the greatest results in terms of photodetector performance, crystallinity, and morphology. The porous Si surface was covered in dense, spherical ZnO nanocrystals, as revealed by Field Emission Scanning Electron Microscope (FESEM) analysis. At longer annealing durations, the crystal size and homogeneity increased. Strong c-axis orientation and high (002) peak intensity were confirmed by XRD patterns, particularly at 60 minutes. At this annealing time, the MSM photodetector showed the best I–V linearity, the lowest leakage current, and the maximum photocurrent (119.1 μA). Additionally, rapid and consistent time-response features were noted. According to the performance table, sensitivity, responsivity (2.50 A/W), and gain peaked at 60 minutes. Annealing improved charge transfer by marginally raising the Schottky barrier height. In general, mild annealing (60 minutes) improved. Annealing improved charge transfer by marginally raising the Schottky barrier height. Overall, the electrical and optoelectronic characteristics of the device were greatly improved by moderate annealing (60 min). These results highlight how these nanostructured materials can be used in renewable energy applications, especially to enhance the performance and efficiency of optoelectronic solar energy conversion and sensing devices.

Keywords: *Annealing, Energy; FESEM, Photodetector, Psi, Renewable; ZnO*

1. INTRODUCTION

Due to their many uses, particularly in ecological monitoring, control systems, and solar astronomy, missile detection, ultraviolet (UV) radiation photo-detectors have attracted a lot of attention recently [1, 2]. UV photo-detectors must have the following characteristics in order to satisfy the demands of diverse applications: quick operational speed, high stability, low cost, IC compatibility, strong linearity, high sensitivity, and a compact design. Due to their innate apparent blindness, wide band gap (WBG) semiconductors should be the best options in this situation [3, 4].

A suitable technique for creating n-PSi with a variety of morphologies is electrochemical etching. Porosity (size, shape, homogeneity, and density distribution), morphology, and fabrication circumstances all have a significant impact on the generated n-PSi's optoelectronic characteristics. These factors can be managed by varying the coating procedure, etching duration, and current density [5, 6. For example, covering the n-PSi layer's top layer can enhance its optoelectronic properties and crystallinity (Yae et al. 2006). In order to do this, a lot of work has been done to increase the effectiveness of PSi-based devices, with a focus on enhancing PSi's electrical and charge carrier transport characteristics [7].

n-PSi is presently being investigated as a precursor for the creation of UV photodetectors (UVPDs) for technological, engineering, and medical applications due to its potent visible and ultraviolet (UV) photoluminescence at room temperature [8-10]. This study investigates the method of maximizing the optoelectronic characteristics of n-PSi for the creation of metal–semiconductor–metal (MSM) UVPDs in light of this demand. In order to enhance the optoelectronic capabilities of formed n-PSi, this work examines the effects of synthesis factors, such as the length of photo electrochemical etching, applied voltage or current, etching solution concentration, and illumination intensity, on the crystallinity and size of the material. Although there have been several studies on how laser irradiation affects PSi's PL and structural characteristics [11-13], no research has looked at how laser irradiation affects PSi-based photo-detectors.

In general, precision processing relies heavily on the Nd:YAG laser. For example, the UV region's pulse laser operation makes it easier to fabricate tiny micro-meter or submicron structures, such catheters, with tiny wires and integrated circuits that are increasingly being used for laser processing. The inherent benefits of nanotechnology, such as its faster processing speed and higher resolution, have made it a viable alternative to traditional UV light sources. The Pentium II, for instance, has a CPU that is 0.25 micron in size, whereas the more recent and sophisticated generations of microprocessors have sizes ranging from 0.13 to 0.18 micron [14-16]. Compared to current etching and electroforming methods, Nd:YAG laser processing offers several advantages at high pulse repetition rate and short pulse width. Additionally, these traditional methods are typically used by the semiconductor industry to create various micro-optical components [17, 18].

As a result, it is anticipated that connecting silicon with a wide band gap (WBG) semiconductor will produce the requisite performance metrics. One WBG in semiconductors has a direct band gap is ZnO [19] and could be utilized to find UV radiation [20]. The produced polycrystalline of ZnO as thin film for UV detectors have thus far shown low photo-responsivity and slow response times in the range of several minutes because of the prolonged lifespan of the photocarriers [21, 22]. The surface traps with deep level of the one-dimensional ZnO nanostructures might be responsible for these distinctive properties [23]. Photo responsiveness of ZnO UV detectors. [24], Despite the fact that ZnO UV detectors have been the subject of countless investigations, was enhanced by changing the surfaces by coating of ZnO thin films by various polymer types positively enhanced the photo responsivity of the detector [24, 25].

Additionally, one claim that covering the ZnO film surface with polyamide nylon enhanced by a factor of four while keeping a responsiveness time of only a few seconds [26]. We want to carefully analyze the potential for producing ZnO nanofilms on PSi substrates and evaluate how well they perform UV pho-todetection. It was shown that ZnO nanofilms put atop a layer of porous silicon considerably increased their resistivity, which increased their response in the UV area. Nevertheless, very few research have investigated how laser irradiation impacts porous silicon's optical and structural characteristics [13].

This research is dedicated to showing how thermal photons and laser annealing affect the performance of n-PSi/ZnO photodiodes. The laser-annealed photodiodes feature fast reaction and recovery times and excellent photo-responsivity.

2. METHODOLOGY AND MATERIALS

2.1. Creating a Porous Silicon Layer on a Silicon Substrate

During this study, n-PSi was developed (at 27° C) on an n-type Si (111) chip of 1.5 cm by 1.5 cm, with a 1 cm^2 etched region chosen for the substrate. Electro-photochemical etching was used to create n-PSi layer, which had three samples with different thicknesses of approximately 9.6, 28.71, and 62.92 μm. The varied direct current densities used were 15, 30, and 45 mA/cm^2. Following research [27], By shining via 50 W for 30 minutes, samples were heated. As previously stated by Pap et al., this heat treatment mediated by light exposure might enable us to obtain the ideal seed layer. [28, 29] and other researchers. Initial findings regarding the etched n-PSi layer's crystal structure, surface shape, and optical characteristics have been published elsewhere [30]. The Si chip substrates were cleaned using the standard method recommended by Radio Corporation of America process (RCA) cleaning to get rid of the oxide layer and impurities [31]. We started with the organic impurities were eliminated by submerging the Si substrates at 80 °C for 5 min in a liquid including 4:2:1 ratios of water, hydrogen peroxide, and nitrous oxide. Then, the tiny coating layer of oxide was removed with submerging these samples in a 30:1 solution of H_2O and HF for 15 seconds at room temperature. Lastly, these substrates were immersed at 80 °C for 5 min in a mix liquid of water, hydrogen peroxide, and HCl in a ratios of 5:1:1 to eliminate the atomic/ionic contaminations.

2.2. Electro-Photochemical Etching's Use to Build the n-PSi Layer

Si chip underwent cleaning. The n-PSi network was formed in a specially built cell as shown in Fig. 1 using photo-electrochemical etching at RT. Teflon was used to make it, and the Si wafer that served as the substrate sealed a circular opening at the bottom. The fundamental design of the cell was containing two-electrode configuration with a silicon wafer work as anode and a platinum (Pt) wire used as cathode. To enable electron conduction inside the solution, The HF solution of (48%), ethanol (C2H5OH) solution with (99.9%), and hydrogen peroxide (H2O2) solution (35%) were combined in a 2:1:1 volume (ml) ratio with the silicon wafer within. The current density was 15 mA/cm2 to create the n-PSi layer while the etching duration time was set at 30 minutes. To utilize the samples to create the MSM PD shown in Fig.2, they were cleaned in ethanol, allowed to dry naturally, and then coated in a coating that was photo-resistant. The PSi layer was covered with the mask directly before being shined with UV light for 50 seconds to create the pattern.

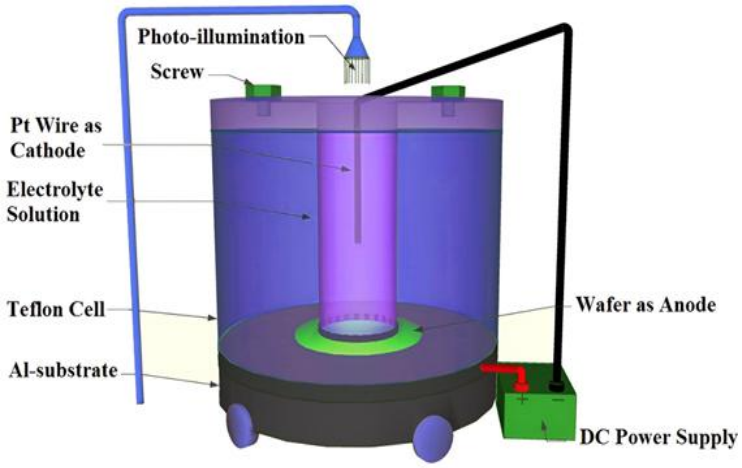

Figure 1. The photo-electrochemical etching method's experimental setup.

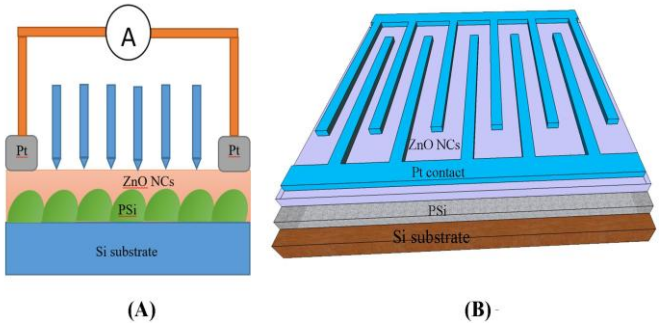

Figure 2. Fabricated MSM photo-detector n-PSi/ZnO NCs (a) Device cross section (b) device diagram.

2.3. Using a Nd-YAG Laser Pulse to Anneal Layers of n-PSi/ZnO NCs

The Nd:YAG laser is work at 1064 nm to annealed the devices and providing 350 mJ of laser energy over 10 pulses. A 10 cm focal length lens was used to concentrate a 10 ns pulse with 30, 60, and 90 minute durations on the target. Effect of the Nd:YAG laser on the processing of Si because the energy of the photons is equal to the energy of the Si bandgap.

3. RESEARCH RESULTS AND DISCUSSION

3.1. FESEM analysis of n-PSi/ZnO NCs

The film of n-PSi/ZnO NCs was heated at 700 °C for 30, 60, and 90 min in Fig. 3 before being exposed to Nd:YAG laser pulses with a 10 ns pulse width and 40 W/cm2 laser intensity. The composite NCs have dimensions of 63.86, 78.39, 73.27, and 51.36 µm, respectively, for annealing durations of 30, 60 and 90 min. The samples' morphological characterisation supports the finding that crystalline size converge with rising of annealing time [22]. It is evident that the surface of n-PSi/ZnO NCs is not significantly influenced by the synthesis time. Surface investigation of the n-PSi/ZnO NCs constructs was done using X-ray microanalysis and FESEM in the elastically reflected electrons mode. Various FESEM pictures reveal a thin layer of nanocrystalline ZnO deposited as spherical dots that almost completely cover the n-PSi layer that has been etched.

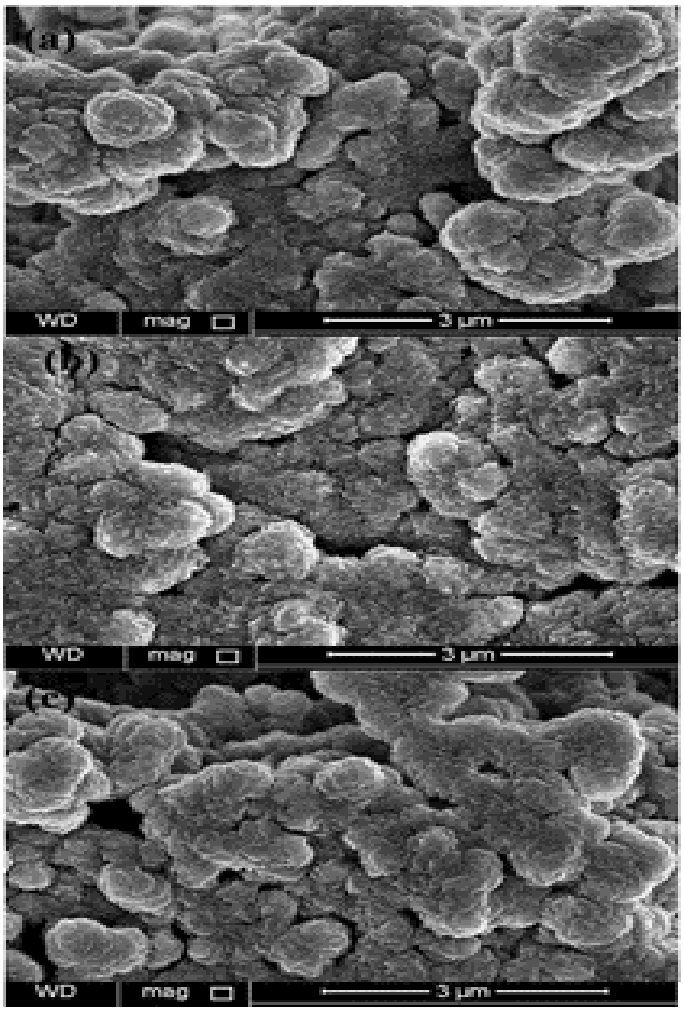

Figure 3. FESEM photos of the annealed n-PSi/ZnO NCs samples at 10 ns pulse width (a) 30 min, (b) 60 min , and (c) 90 min

3.2. XRD Measurement

Fig. 4 displays the thin-film n-PSi/ZnO NCs' XRD patterns. According to JCPDS Card No. 01-089-1397, The three peaks at 2θ = 31.76°, 34.48°, and 36.26° are reflected from (111), (002), and (101) respectively, of the ZnO structure phase. There were further three other summits. PSi is the substrate. It should be emphasized that no clear peaks exist for any other phases or contaminated phases. Reflection (002) is indicated by higher intensity. indicates the c-axis orientation is the preferred development direction for ZnO NCs. because to improved crystallization of ZnO NCs[34], or maybe due to nucleation and differential growth, the strength of the (002) peak increased at 30 and 60 min while it slightly dropped at 90 min annealing. Due to the free density of surface energy along the (002) direction is the lowest in ZnO crystals, ZnO NCs favor development along this direction[36]. Between 31.38 and 36.16°, a complicated XRD pattern that is characteristic of the PSi substrate occurs[25]. Scherrer's formula 1 was used to compute the crystallite size (D)[37-39],

$$D=0.9\lambda/(\beta \cos\theta) \quad (1)$$

where λ is the wavelength of incident X-ray of 1.5406 Å, the full width at half maximum (FWHM) is β and θ is the Bragg angle. The size of the n-PSi/ZnO NCs annealed for 30, 60, and 90 minutes obtained within 15–16 nm of one another shown in Table(1).

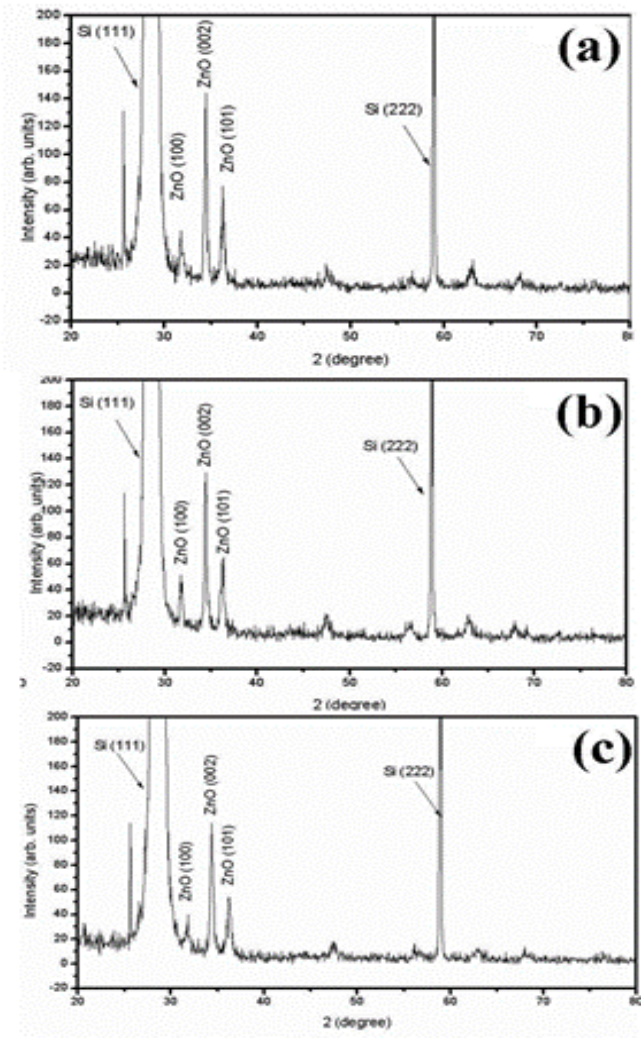

Figure 4. XRD result of n-PSi/ZnO NCs the laser annealed at 10 ns pulse width (a) 30 min, (b) 60 min , and (c) 90 min.

Table 1 XRD result of n-PSi/ZnO NCs the laser annealed at 10 ns pulse width (a) 30 min, (b) 60 min , and (c) 90 min

Sample	***2θ* (002) (°)**	**FWHM (°)**	***a* (nm)**	***c* (nm)**	***D* (nm)**
(a)	34.02	0.56	0.326	0.526	15.5
(b)	34.00	0.578	0.328	0.527	15
(c)	33.95	0.55	0.330	0.528	15.7

3.3. I-V Properties of the MSM Photo-detector Device

When exposed to 1.5 mW/cm2 of 530 nm Visible light in the dark, a bias voltage in the (+5 V to -5 V) range was used to evaluate the I-V characteristics of the MSM UV photo-detector. There is a Shottky contact between the ZnO NCs networks and the Pt electrodes which can be proofed by the linear I-V characteristics that could be found under forward and reverse bias circumstances. The photo-detector's measured dark current at -4 V of bias was 8.07 A, which was less than what previous researchers had found [40, 41]. The low dark current actually made it possible to re-evaluate the detector's ratio of signal to noise (S/N) [41, 42]. At UV light, the device's current was 119.1 nA Fig.(5). The strong photocurrent obtained due to the high crystallization and substantial surface area to volume ratio. Overall, it was shown that a 60-minute moderate healing period increased the device's I-V responsiveness. In turn, this reasonable amount of time contributes to an increase in anodization current density, which may improve the performance of the suggested photo-detector. In terms of structure, MSM is two Schottky contacts linked back-to-back. Because of how the connections are set up, reverse and forward bias are possible with biasing voltages between 5 V and +5 V.

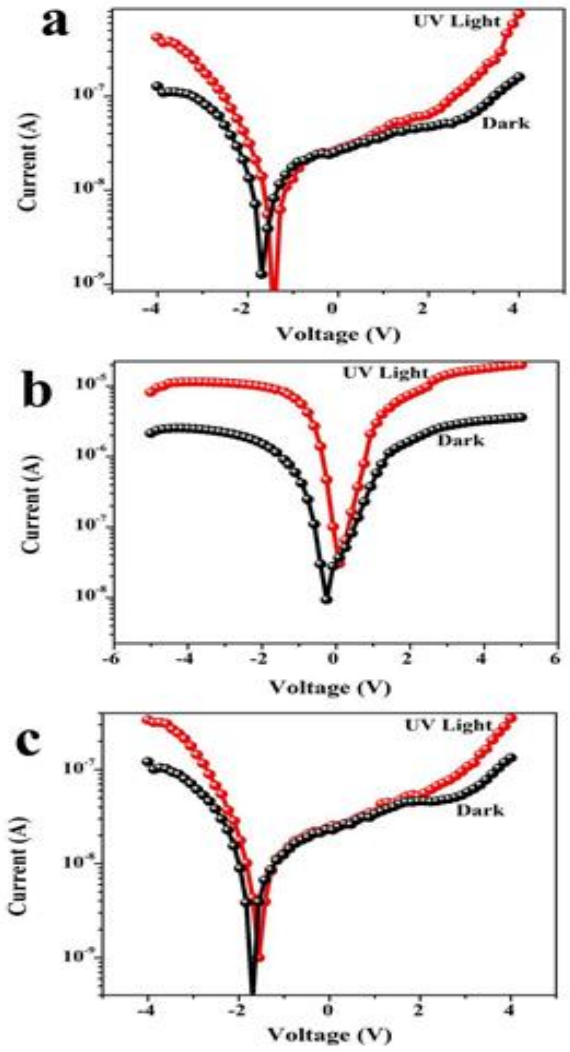

Figure 5. I-V curves for the UV photodetector generated with an n-PSi specimen that had been annealed for (a) 30 minutes, (b) 60 minutes, and (c) 90 minutes, respectively.

In general, raising the bias voltage increases the MSM photodetector's sensitivity. It was determined that the photodetector's limited current flow brought on by the space charge region was the reason which make MSM device's current was close to be below 0.5 V. Additionally, the n-PSi layer absorbed light in the higher voltage zone, producing more h-e pairs inside the region. Then, the electric field evolved inside the space charge region using a high bias voltage. The charge carriers will separate, resulting in increased a high carrier mobility and thermionic emission. The current will grow exponentially when the applied voltage exceeds the potential barrier. The bias voltage provided the electron with enough energy to cross the barrier height and initiate a diffusion current [43], the holes and electrons will be drift in opposite directions. This mechanism, which creates of the photocurrent in the outside contact. In addition, the circuit's electron influx converted optical impulses into electrical signals, successfully realizing the photodetector. This result provided a clear illustration of how current densities affect the I-V characteristics of the MSM PD.

The specimen current, which was noticeably high compared to other specimens, was connected to the moderate resistivity, mobility, and Schottky barrier height of the PD. As a result of the lengthy preparation period of 90 minutes, the sample prepared at 30 mints had low concentration and low current whereas the sample made at 90 mints had the maximum leakage current [35]. The sample that was created after 60 minutes had the lowest leakage current value, demonstrating enhanced electrical characteristics. The claim states that an MSM photodetector was created that was equivalent to Hadjersi's stated devices in the visible region and had optical transparency [36] and some researchers [34]. The device's improved performance was controlled by the Schottky high barrier value and the ideality factor.

On the basis of an n-PSi specimen that was handled with the same current and bias applied at intervals of 20 s, Fig. 6 show the time dependent response graph of the built UV PD (at -4 V). At these bias voltages, the photodetector displayed good stability and repeatability behaviour. The time-dependent current response displayed rectangular fluctuation, and the photocurrent was reproducible and

steady. From these current-time graphs, it was determined that the rise times and the recovery of these PDs were quite quick during the rising period, the current can rise between 10% and 90% of its saturation state, as the current can climb from 10% to 90% of its saturation value during the recovery time.

The MSM photodetector's recovery time, responsiveness, response time, and sensitivity are listed in Table 2 for the two distinct 0.5 and 1.0 V bias voltage. These values are as a function in the current density. The outcomes were comparable to prior discoveries [1, 38]. The huge surface of photoactive areas and the excellent ZnO structures produced by varying current density were linked to the speedily photo response and recovery that was seen, suggesting that such PZnO samples might be used in high-speed operations. The rising in current density increased the photodetector's responsiveness, sensitivity, and gain. The aggregation of many carriers on the p-GaN thin films under visible light illumination was blamed for the improvement in photo detection ability.

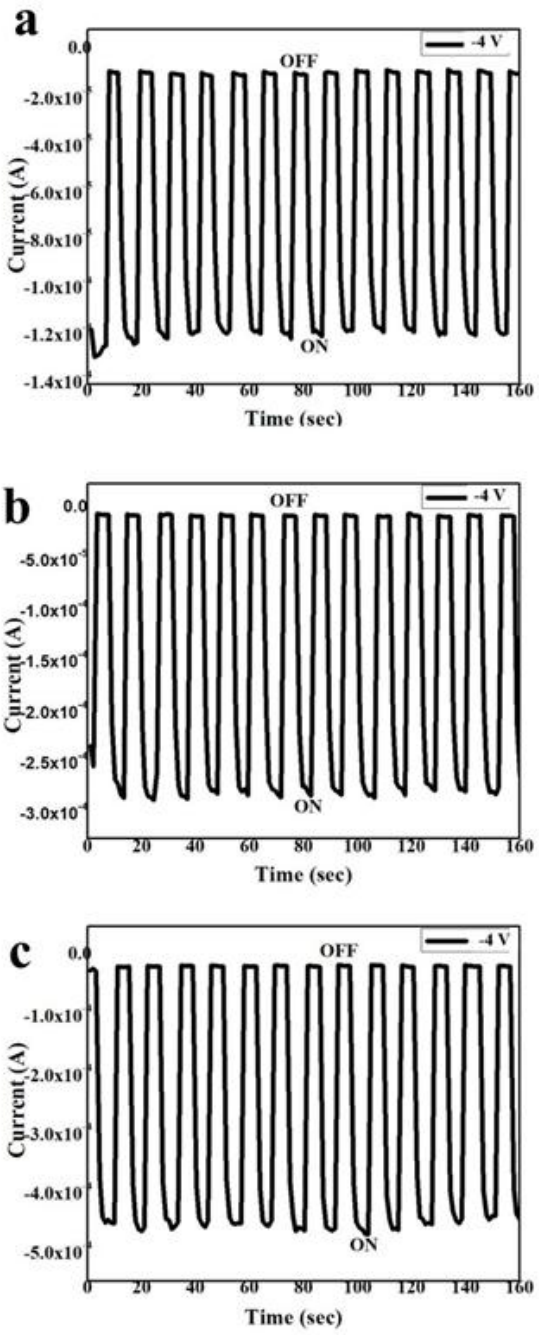

Figure 6. Time response of the UV n-PSi photodetector prepared at different annealing time (a). 30 min, (b) 60 min and (c). 90min.

Table 2 The photoelectrical characteristics of the MSM PD are affected by the annealing time

Wavelength (nm)	Sample	Bias voltage (V)	Response time (sec)	Recovery time (sec)	Sensitivity (%)	Responsivity (A/W)	Gain
530	30min	0.5	0.49	0.47	25	0.50	2.09
		1	7.60	4.00	13		1.11
530	60 min	0.5	0.47	0.43	119	0.80	2.15
		1	0.52	0.45	152		2.50
530	90 min	0.5	0.46	0.43	45	0.35	1.74
		1	0.52	0.35	43		1.33

Utilizing the idea of thermionic emission-diffusion [44-46], the ideality factor (n) and the Schottky height barrier (Φ_B) can be expressed as:

$$I = I_0 \, exp\left(\frac{qV}{nkT}\right)\left[1 - exp\frac{-qV}{kT}\right] \quad (2)$$

$$I_0 = ART^2 exp\left[\frac{-\Phi_B}{kT}\right] \quad (3)$$

where q is the electronic charge, A is the area of the Schottky contact (0.25 cm2), k is the Boltzmann constant, R is the effective Richardson coefficient (112 A/cm^2.K2), T is the temperature, and Io is the saturation current. The value of B was determined using the I-V curve. The I0 value for the proposed UV photo-detector was evaluated using Eq. (3) change with different etching times.

The n-PSi/ZnO NCs specimens worked in the device had average values of 0.70 eV, 0.72 eV, and 0.73 eV, respectively, at varied annealing times of 30 minutes, 60 minutes, and 90 minutes. Surface roughening, which significantly contributed to the improvement of the electrical characteristics at the moderate surface between the n-PZnO and Pt, was attributable to little variation in the B values at various annealing times [47]. The Fermi level moved toward the valence band while the current leaks decreased when B increased from high porosity at high current density. Higher density of interfacial states may be correlated with high values of the ideality factor [48]. It was accepted that this enhancement was mostly due to the samples' two heterojunctions, one at the PSi substrate contact and the other at the n-PZnO border [49, 50]. In addition, as already mentioned, the frequency of inhomogeneous barrier height can rise [40].

3.4 The Photoconduction Mechanism

The mechanism of photoconduction throughout the n-PSi diagram of energy band under UV and dark illumination is schematically shown in Fig. 7. In the absence of light, the oxygen molecules got absorbed onto the n-PSi layer's surface, where they then grabbed free electrons to form ions (Fig. 9(a)). You can sum up the chemical reaction process as [51]:

$$O_{2(g)} + e^- \rightarrow O_{2^-(ad)} \quad (4)$$

Due to the ability of these oxygen ions to create a depletion region, the conductivity of the n-PSi layer was reduced on the other hand, the generation of e-h pairs could occur from exposure to ultraviolet (UV) light with photon energy (hv) larger than the width of the band gap (Eg) of the n-PSi layers [43] via the next process:

$$h\nu \rightarrow e^- + h^+ \quad (5)$$

The Si Nano crystallites' surface may have been targeted by the internal electric field in the depletion zone, which also separated the e-h couplings to allow the recombination between the adsorbed oxygen ions and holes. The following procedure led to the fire the oxygen atoms from the surface of the Si Nano crystallites' because of this process (Fig. 9(b)):

$$h^+ + O^-_{2(ab)} \rightarrow O_{2(g)} \quad (6)$$

In the meantime, the photo-generated electrons contributed to the photoconduction by filling the conduction band (CB). Therefore, the rising of electrons concentration may result in an improvement in conductivity. The large photocurrent was primarily caused by the creation of charge carriers (e-h) in the n-PSi crystallite surface's depletion zone as a result of light [52].

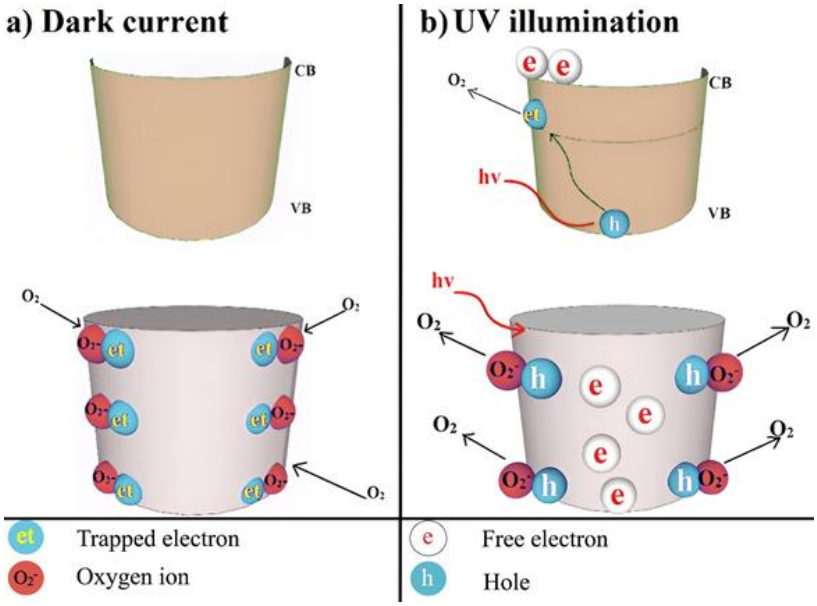

Figure 7. Diagram showing the PD in n-PSi over the energy band in two different lighting conditions: (a) complete darkness, and (b) illumination with UV light [8].

$$S(\%) = \frac{Iph-Id}{Id} \times 100 \quad (7)$$

where I_{ph} is the photo current, the dark current is Id . It was found that the photocurrent for the samples grown at constant anodization current densities and predictable during each on/off period. Table 2 shows that at annealing time of 30, 60, and 90 min, the response time were found to be 0.49 s, 7.6 s, and 0.47 s, 0.52 s 0.46s, and0.52 s respectively. The n-PSi sample generated at 30min had the quickest reaction and recovery times, outperforming the previously reported one [53, 54]. The high photoactive surface area, good quality, and defect-free status of the generated n-PSi specimens were credited with the quick reaction that was seen at maximal anodization current. Additionally, the quick response was connected to the photo-generated carriers' quick transit time and extended lifetime [55]. On the other hand, rich oxygen adsorption at grain boundaries and the surface were associated with the photo-detector's poor response time [52].

Alternatively, you may insert the whole text or parts you previously prepared by using on the 'Insert' menu of Word® the option 'File…'. In that case take care to retain or re-insert the above mentioned section breaks. After the file is inserted, you can style it by placing the cursor in each paragraph and clicking the required style on the drop-down menus.

The PD device was evaluated using a different measure known as the Responsivity (R, in A/W), [56, 57] via:

$$R = \frac{Iph}{Pinc} = \frac{Iph}{E.A} \quad (8)$$

where E is the illumination photon's energy, as determined by a typical UV power meter. The photo-detector's responsiveness was assessed in the wavelength range of 300-900 nm at RT and 3 V as a bias voltage. The proposed MSM device's anodization current density-dependent photo response is shown in Fig. 8 shows the bias voltage (VB), the peak responsivity (Rp), and the highest (peak) wavelength of the diode response (p). For the device fabricated at varied times of 30, 60, and 90 min, respectively, the responsivity spectra featured a noticeable visible peak located at 60 min. The increase in time annealing the photo detector's overall responsiveness. The measured values of responsiveness for time annealing of 30, 60, and 90 min were 3.89, 4.10, and 3.27 A/W, respectively [36]. It was found that the strong peak at 365 nm, which was previously seen in an Au-Si-based device, was present in the higher platinum connections [58].

When the anodization current density was higher and the porosity was higher, In the depletion area, more e-h pairs were generated, improving the responsivity at lower wavelengths. This was anticipated since the wavelength-dependent penetration depth might decrease absorption in the Si substrate while in the same time enhancing the depletion zone. When a result, when the wavelength was decreased, more e-h pairs were generated in the depletion zone. Further investigation found that at shorter wavelengths (blue and near UV), the light responsiveness was significantly diminished. This was verified by the photons' inability to reach the depletion zone due to their absorption in the n-PSi layer [59] which was consistent with other findings [60, 61]. Up until 530 nm, the photocurrent grew in relation to wavelength and then abruptly decreased in the visible region. UV light's penetration depth shrank as illumination light's wavelength shrank due to an increase in the absorption coefficient. The number of carriers increased as a result of this situation. We were able to acquire a greater value of responsiveness than Hadjersi et al. [58] and Al-Jumaili et al. [28].

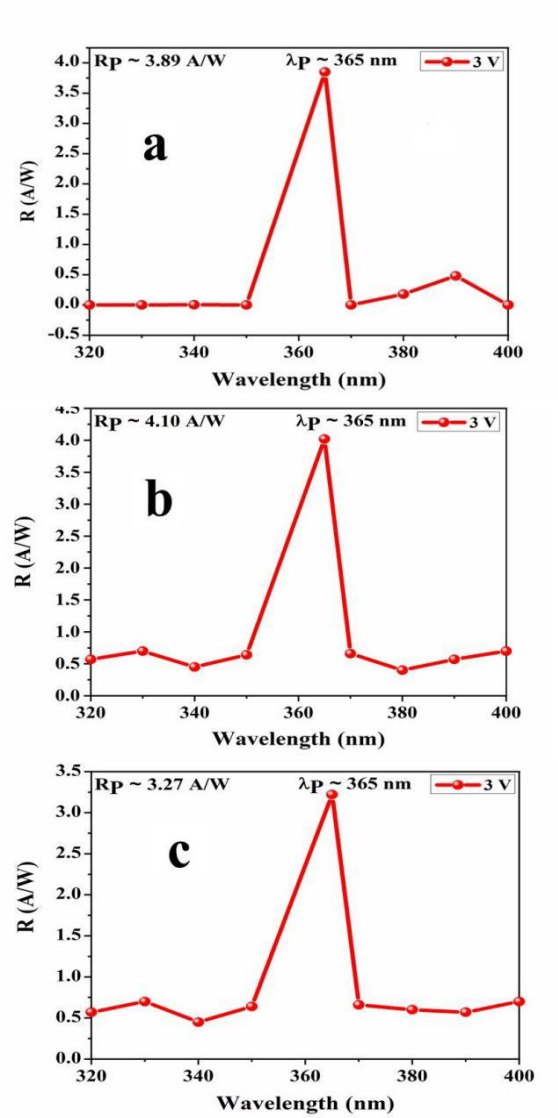

Figure 8. Annealing time dependent responsivity of the MSM device at 5 V of bias for photo-detectors annealed at (a) 30min, (b) 60 min and (c) 90 min.

The I_{ph} generated for each amount of incident power (Pin) was used to define the photo-detector's quantum efficiency (η) [62-64]:

$$\eta\ (\%) = \frac{Iph}{q}\ \frac{hv}{Pin} \tag{9}$$

The photo-detector's quantum efficiency (η) may be expressed as follows in terms of responsiveness (R): [65-68]:

$$\eta\ (\%) = \frac{hc}{Gq\lambda} \mathrm{R} = \frac{1.24\ R}{g\ \lambda\ (\mu m)} \tag{10}$$

where g denotes the current gain of device. The G value was computed using the ratio of electrons gathered in the dark per unit time to the photons absorbed to create photoelectron per unit time [46, 47]. The value of G was expressed from the I-V curve via equation 11:

$$G = \frac{Iph}{Id} \tag{11}$$

Under irradiation at 530 nm (1.5 mW/cm2) and 0.5 V as bias voltage, the predicted value of G was 2.5. The optically response of the PD to a UV pulse with a wavelength of 530 nm and an intensity of 1.5 mW/cm2 was measured at various bias voltages ranging from 0.5 to 1 V in order to assess the PD's reversibility

ACKNOWLEDGMENTS

This work was funded by the University of Jeddah, Jeddah, Saudi Arabia, under grant No. (UJ-22-DR-91). The author, therefore, acknowledge with thanks the University of Jeddah for its technical and financial support.

REFERENCE

[1] Lei Luo, Yanfeng Zhang, Samuel S Mao, and Liwei Lin, "Fabrication and characterization of ZnO nanowires based UV photodiodes," Sensors and Actuators A: Physical **127** (2), 201-206 (2006); Eva Monroy, Franck Omnès, and FJSS Calle, "Wide-bandgap

semiconductor ultraviolet photodetectors," Semiconductor science and technology **18** (4), R33 (2003).

[2] Lei Shi and Stoyan Nihtianov, "Comparative study of silicon-based ultraviolet photodetectors," IEEE Sensors Journal **12** (7), 2453-2459 (2012).

[3] J Dian, A Macek, D Nižňanský, I Němec, V Vrkoslav, T Chvojka, and I Jelınek, "SEM and HRTEM study of porous silicon—relationship between fabrication, morphology and optical properties," Applied Surface Science **238** (1-4), 169-174 (2004).

[4] Roaa A. Abbas, Evan T. Salim & Rana O. Mahdi, Deposition time effect on copper oxide nano structures, an analysis study using chemical method, J Mater Sci: Mater Electron 35, 427 (2024). https://doi.org/10.1007/s10854-024-12143-0

[5] Salah E El-Zohary, MA Shenashen, Nageh K Allam, T Okamoto, and M Haraguchi, "Electrical characterization of nanopolyaniline/porous silicon heterojunction at high temperatures," Journal of Nanomaterials **2013** (1), 568175 (2013).

[6] Khawla S khashan, Rana O Mahdi, Ban A. Badr, Farah Mahdi, Preparation and characterization of ZnMgO nanostructured materials as a photodetector, Journal of Physics: Conference Series 1795 (2021) 012008. doi:10.1088/1742-6596/1795/1/012008

[7] Asad A Thahe, Noriah Bidin, Z Hassan, Hazri Bakhtiar, MA Qaeed, Mohamed Bououdina, Naser M Ahmed, Zainal A Talib, Mohammed A Al-Azawi, and Hasan Alqaraghuli, "Photo-electrochemically synthesized light emtting nanoporous silicon based UV photodetector: influence of current density," Materials Research Express **4** (11), 116203 (2017).

[8] Asad A Thahe, Basant A Ali, Hazri Bakhtiar, MB Uday, Z Hassan, Mundzir Abdullah, MA Qaeed, Hasan Alqaraghuli, Hussein Abd Zaidan, and Nageh K Allam, "Laser annealing enhanced the photophysical performance of Pt/n-PSi/ZnO/Pt-based photodetectors," Solid-State Electronics **171**, 107821 (2020).

[9] Aseel A. Hadi, Juhaina M. Taha, Rana O. Mahdi, Khawla S. Khashan, Influence of laser pulse on properties of NiO NPs prepared by laser ablation in liquid, AIP Conf. Proc. 2213, 020308 (2020) https://doi.org/10.1063/5.0000115

[10] V Yu Timoshenko, Th Dittrich, I Sieber, J Rappich, BV Kamenev, and PK Kashkarov, "Laser-Induced Melting of Porous Silicon," physica status solidi (a) **182** (1), 325-330 (2000).

[11] AA Chistyakov, VA Karavanski, MB Kuznetsov, GM Voronkova, VV Zuev, and LK Orlova, "On the possibility of controlling the photoluminescence spectrum of nanoporous silicon with laser radiation," Laser physics **10** (4), 881-886 (2000).

[12] Evan T. Salim, Ahmed T. Hassan, Rana O Mahdi, Forat H. Alsultany, Physical Properties of HfO2 Nano Structures Deposited using PLD, IJNeaM, vol. 16, no. 3, pp. 495–510, Oct. 2023.

[13] Leigh T Canham, "Silicon quantum wire array fabrication by electrochemical and chemical dissolution of wafers," Applied physics letters **57** (10), 1046-1048 (1990).

[14] Azzam Y. kudhur, Evan T. Salim, Ilker Kara, Rana O. Mahdi & Raed K. Ibrahim, The effect of laser energy on Cu2O nanoparticles formation by liquid-phase pulsed laser ablation, J Opt 53, 1309–1321 (2024). https://doi.org/10.1007/s12596-023-01319-2

[15] George C John and Vijay A Singh, "Porous silicon: theoretical studies," Physics reports **263** (2), 93-151 (1995).

[16] Hassen H. H.; Salim E. T.; Taha J. M.; Mahdi R. O.; Numan N. H.; Khalid F. G.; Fakhri M. A., Fourier transform infrared spectroscopy and photo luminance results for Zno NPs prepared at different preparation condition using LP-PLA technique, International Journal of Nanoelectronics and Materialsm, 11(Special Issue BOND21) 65-72 (2018)

[17] Sheng-Joue Young, Liang-Wen Ji, Shoou-Jinn Chang, and Yan-Kuin Su, "ZnO metal–semiconductor–metal ultraviolet sensors with various contact electrodes," Journal of crystal growth **293** (1), 43-47 (2006).

[18] Rana O. Mahdi, Aseel A. Hadi, Juhaina M. Taha, Khawla S. Khashan, Preparation of nickel oxide nanoparticles prepared by laser ablation in water, AIP Conf. Proc. 2213, 020309 (2020) https://doi.org/10.1063/5.0000116

[19] JH He, Yen H Lin, Michael E McConney, Vladimir V Tsukruk, Zhong L Wang, and Gang Bao, "Enhancing UV photoconductivity of ZnO nanobelt by polyacrylonitrile functionalization," Journal of Applied Physics **102** (8) (2007).

[20] Jun Zhou, Yudong Gu, Youfan Hu, Wenjie Mai, Ping-Hung Yeh, Gang Bao, Ashok K Sood, Dennis L Polla, and Zhong Lin Wang, "Gigantic enhancement in response and reset time of ZnO UV nanosensor by utilizing Schottky contact and surface functionalization," Applied physics letters **94** (19) (2009).

[21] Noha Samir, Dina S Eissa, and Nageh K Allam, "Self-assembled growth of vertically aligned ZnO nanorods for light sensing applications," Materials Letters **137**, 45-48 (2014).

[22] Roaa A. Abbas, Evan T. Salim & Rana O. Mahdi, Morphology transformation of Cu2O thin film: different environmental temperatures employing chemical method, J Mater Sci: Mater Electron 35, 1057 (2024). https://doi.org/10.1007/s10854-024-12823-x

[23] KW Liu, JG Ma, JY Zhang, YM Lu, DY Jiang, BH Li, DX Zhao, ZZ Zhang, B Yao, and DZ Shen, "Ultraviolet photoconductive detector with high visible rejection and fast photoresponse based on ZnO thin film," Solid-State Electronics **51** (5), 757-761 (2007).

[24] AM Suhail, EK Hassan, SS Ahmed, and MKM Alnoori, "Improvement of the photoresponse of the solar blind ZnO photoconductive UV detector," Journal of Electron Devices **8**, 268-274 (2010).

[25] Fakhri M. A.; Wahid M. H. A.; Badr B. A.; Kadhim S. M.; Salim E. T.; Hashim U.; Salim Z. T., Enhancement of Lithium Niobate nanophotonic structures via spin-coating technique for optical waveguides application, EPJ Web of Conferences, 162, 1004 (2017) 10.1051/epjconf/201716201004

[26] Batool Eneaze B Al-Jumaili, Zainal A Talib, Asmiet Ramizy, Naser M Ahmed, LY Josephine, Suriati B Paiman, Ibrahim B Muhd, and Sinan A Abdulateef, "Responsivity dependent anodization current density of nanoporous silicon based MSM photodetector," Journal of Nanomaterials **2016** (2016).

[27] Andrea Edit Pap, Krisztián Kordás, Jouko VäHäkangas, Antti Uusimäki, Seppo Leppävuori, Laurent Pilon, and Sándor Szatmari, "Optical properties of porous silicon. Part III: Comparison of experimental and theoretical results," Optical Materials **28** (5), 506-513 (2006).

[28] M Abu-Hussein, C Georges, N Watted, and A Azzaldeen, "A clinical study resonance frequency analysis of stability during the healing period," Int J Oral Craniofac Sci 2 (1): 065-071. DOI **10**, 2455-4634.0000 (2016).

[29] Azzam Y. Kudhur, Evan T. Salim, Ilker Kara, Makram A. Fakhri & Rana O. Mahdi, Structural optical and morphological properties of copper oxide nanoparticles ablated using pulsed laser ablation in liquid, J Opt 53, 1936–1945 (2024). https://doi.org/10.1007/s12596-023-01331-6

[30] Karen Reinhardt and Werner Kern, *Handbook of silicon wafer cleaning technology*. (William Andrew, 2008).

[31] Lin Cui, Gui-Gen Wang, Hua-Yu Zhang, Rui Sun, Xu-Ping Kuang, and Jie-Cai Han, "Effect of film thickness and annealing temperature on the structural and optical properties of ZnO thin films deposited on sapphire (0001) substrates by sol–gel," Ceramics International **39** (3), 3261-3268 (2013).

[32] Forat H Alsultany, Naser M Ahmed, and MZ Matjafri, "Effects of CW CO 2 laser annealing on indium tin oxide thin films characteristics," Soft Nanoscience Letters **4** (04), 83 (2014).

[33] Muhsien M. A.; Salem E. T.; Agool I. R.; Hamdan H. H., Gas sensing of Au/n-SnO2/p-PSi/c-Si heterojunction devices prepared by rapid thermal oxidation, Applied Nanoscience (Switzerland), 4(6), 719-732 (2014) 10.1007/s13204-013-0244-7

[34] J Lee, W Gao, Z Li, M Hodgson, J Metson, H Gong, and U Pal, "Sputtered deposited nanocrystalline ZnO films: a correlation between electrical, optical and microstructural properties," Applied Physics A **80**, 1641-1646 (2005).

[35] R Noonuruk, W Techitdheera, and W Pecharapa, "Characterization and ozone-induced coloration of ZnxNi1− xO thin films prepared by sol–gel method," Thin solid films **520** (7), 2769-2775 (2012).

[36] MA Qaeed, K Ibrahim, KMA Saron, MS Mukhlif, A Ismail, Nezar G Elfadill, Khaled M Chahrour, QN Abdullah, and KSA Aldroobi, "New issue of GaN nanoparticles solar cell," Current Applied Physics **15** (4), 499-503 (2015).

[37] Fakhri M. A.; Numan N. H.; Alshakhli Z. S.; Dawood M. A.; Abdulwahhab A. W.; Khalid F. G.; Hashim U.; Salim E. T., Physical investigations of nano and micro lithium-niobate deposited by spray pyrolysis technique, AIP Conference Proceedings, 2045, 20015 (2018) 10.1063/1.5080828

[38] Husnen R Abd, Y Al-Douri, Naser M Ahmed, and U Hashim, "Alternative-current electrochemical etching of uniform porous silicon for photodetector applications," Int. J. Electrochem. Sci **8**, 11461-11473 (2013).

[39] Mohammed D. A.; Kadhim A.; Fakhri M. A., The enhancement of the corrosion protection of 304 stainless steel using Al2O3 films by PLD method, AIP Conference Proceedings, 2045, 20014 (2018) 10.1063/1.5080827

[40] Batool Eneaze B Al-Jumaili, Zainal A Talib, Asmiet Ramizy, Naser M Ahmed, LY Josephine, Suriati B Paiman, Ibrahim B Muhd, and Sinan A Abdulateef, "Responsivity Dependent Anodization Current Density of Nanoporous Silicon Based MSM Photodetector," Journal of Nanomaterials **2016**, 3 (2016).

[41] Xuehui Gu, Min Zhang, Fanxu Meng, Xindong Zhang, Yu Chen, and Shengping Ruan, "Influences of different interdigital spacing on the performance of UV photodetectors based on ZnO nanofibers," Applied Surface Science **307**, 20-23 (2014).

[42] AF Abd Rahim, MR Hashim, and NK Ali, "High sensitivity of palladium on porous silicon MSM photodetector," Physica B: Condensed Matter **406** (4), 1034-1037 (2011).

[43] Tawfiq Z. H.; Fakhri M. A.; Adnan S. A., Photonic Crystal Fibres PCF for Different Sensors in Review, IOP Conference Series: Materials Science and Engineering, 454(1), 12173 (2018) 10.1088/1757-899X/454/1/012173

[44] Asad A Thahe, Hazri Bakhtiar, Basant A Ali, Z Hassan, Nroiah Bidin, Mohamed Bououdina, MA Qaeed, Zainal A Talib, Mohammed A Al-Azawi, and Hasan Alqaraghuli, "Photophysical performance of radio frequency sputtered Pt/n-PSi/ZnO NCs/Pt photovoltaic photodetectors," Optical Materials **84**, 830-842 (2018).

[45] JM Perez, J Villalobos, P McNeill, J Prasad, R Cheek, J Kelber, JP Estrera, PD Stevens, and R Glosser, "Direct evidence for the amorphous silicon phase in visible photoluminescent porous silicon," Applied Physics Letters **61** (5), 563-565 (1992).

[46] D Dimova-Malinovska and M Nikolaeva, "Transport mechanisms and energy band diagram in ZnO/porous Si light-emitting diodes," Vacuum **69** (1), 227-231 (2002).

[47] Fakhri M. A.; Bader B. A.; Khalid F. G.; Numan N. H.; Abdulwahhab A. W.; Hashim U.; Salim E. T.; Munshid M. A.; Salim Z.T., Optical and morphological studies of LiNbO3 nano and micro photonic structural, AIP Conference Proceedings, 2045, 20017 (2018) 10.1063/1.5080830

[48] Ahmed Chouket, Boutheina Cherif, Nasr Ben Salah, and Kamel Khirouni, "Optical and electrical properties of porous silicon impregnated with Congo Red dye," Journal of Applied Physics **114** (24), 243105 (2013).

[49] Mazhar Ali Abbasi, Zafar Hussain Ibupoto, Azam Khan, Omer Nur, and Magnus Willander, "Fabrication of UV photo-detector based on coral reef like p-NiO/n-ZnO nanocomposite structures," Materials Letters **108**, 149-152 (2013).

[50] Minuk Jo, Ki Jung Lee, and Sang Sik Yang, "Sensitivity improvement of the surface acoustic wave ultraviolet sensor based on zinc oxide nanoparticle layer with an ultrathin gold layer," Sensors and Actuators A: Physical **210**, 59-66 (2014).

[51] Doaa A. Mahmoud, Evan T. Salim, Rana O. Mahdi, A. Mindil, Subash C. B. Gopinath & Motahher A. Qaeed, Laser Ablation of Tungsten Metal for Au@WO3 Core-Shell Formation: A Characterizing Study at Different Laser Fluences, Plasmonics (2024). https://doi.org/10.1007/s11468-024-02607-8

[52] Abbas M Selman and Z Hassan, "Highly sensitive fast-response UV photodiode fabricated from rutile TiO 2 nanorod array on silicon substrate," Sensors and Actuators A: Physical **221**, 15-21 (2015).

[53] Naser M Ahmed, Z Hassan, Naif Alhardan, Yarub Aldouri, MJ Jassim, Muhammad Anis Ibnu Hajar, SK Mohd Bakhdri, and NA Ahmad Zaini, presented at the AIP Conference Proceedings, 2012 (unpublished).

[54] HI Abdulgafour, Z Hassan, FK Yam, K Al-Heuseen, and Y Yusof, "Enhancing photoresponse time of low cost Pd/ZnO nanorods prepared by thermal evaporation techniques for UV detection," Applied Surface Science **258** (1), 461-465 (2011).

[55] Fakhri M. A.; Abdulwahhab A. W.; Dawood M. A.; Raheema A. Q.; Numan N. H.; Khalid F. G.; Wahid M. H. A.; Hashim U.; Salim E. T., Optical investigations of nano lithium niobate deposited by spray pyrolysis technique with injection of Li2CO3 and Nb2O5 as raw materials, International Journal of Nanoelectronics and Materials, 11(Special Issue BOND21), 103-108 (2018)

[56] Liang Guo, Hong Zhang, Dongxu Zhao, Binghui Li, Zhenzhong Zhang, Mingming Jiang, and Dezhen Shen, "High responsivity ZnO nanowires based UV detector fabricated by the dielectrophoresis method," Sensors and Actuators B: Chemical **166**, 12-16 (2012).

[57] Alper Ercan and Kyriaki Minoglou, "A model to estimate QE/MTF of thinned, back-side illuminated image sensors," Optical and Quantum Electronics **47** (5), 1267-1282 (2015).

[58] T Hadjersi and N Gabouze, "Photodetectors based on porous silicon produced by Ag-assisted electroless etching," Optical Materials **30** (6), 865-869 (2008).

[59] Jehan A. Saimon, Suzan N. Madhat, Khawla S. Khashan, Azhar I. Hassan, Rana O. Mahdi, Rafah A. Nasif, Synthesis of CdxZn1-xO nanostructure films using pulsed laser deposition technique, AIP Conf. Proc. 2045, 020003 (2018) https://doi.org/10.1063/1.5080816

[60] AV Brodovoi, VA Brodovoi, VA Skryshevskyi, SG Bunchuk, and LM Khnorozok, "Photoelectric properties of metal-porous silicon-silicon planar heterostructures," Semiconductor Physics, Quantum Electronics & Optoelectronics **5** (4), 395-397 (2002).

[61] Yung-Huang Chang, Chien-Min Liu, Yuan-Chieh Tseng, Chih Chen, Chia-Chuan Chen, and Hsyi-En Cheng, "Direct probe of heterojunction effects upon photoconductive properties of TiO2 nanotubes fabricated by atomic layer deposition," Nanotechnology **21** (22), 225602 (2010).

[62] Zainab T. Hussain, Khawla S. Khashan, Rana O. Mahdi, Characterization of cadmium oxide nanoparticles prepared through Nd:YAG laser ablation process, Materials Today: ProceedingsVolume 42, Pages 2645 – 26482021. https://doi.org/10.1016/j.matpr.2020.12.594

[63] NK Hassan, MR Hashim, and Nageh K Allam, "Low power UV photodetection characteristics of cross-linked ZnO nanorods/nanotetrapods grown on silicon chip," Sensors and Actuators A: Physical **192**, 124-129 (2013).'

[64] Alsultany F. H.; Alhasan S. F. H.; Salim E. T., Seed Layer-Assisted Chemical Bath Deposition of Cu2O Nanoparticles on ITO-Coated Glass Substrates with Tunable Morphology, Crystallinity, and Optical Properties, Journal of Inorganic and Organometallic Polymers and Materials, 31(9), 3749-3759 (2021) 10.1007/s10904-021-02016-y

[65] Fakhri M. A.; Wahid M. H. A.; Kadhim S. M.; Badr B. A.; Salim E. T.; Hashim U.; Salim Z. T., The structure and optical properties of Lithium Niobate grown on quartz for photonics application, EPJ Web of Conferences, 162, 1005 (2017) 10.1051/epjconf/201716201005

[66] NH Al-Hardan, MJ Abdullah, NM Ahmed, FK Yam, and A Abdul Aziz, "UV photodetector behavior of 2D ZnO plates prepared by electrochemical deposition," Superlattices and Microstructures **51** (6), 765-771 (2012).

[67] Khawla S. Khashan, Aseel A. Hadi, Rana O. Mahdi & Doaa S. Jubair, Aluminum-doped zinc oxide nanoparticles prepared via nanosecond Nd: YAG laser ablation in water: optoelectronic properties, Opt Quant Electron 56, 125 (2024). https://doi.org/10.1007/s11082-023-05630-x

[68] Abdul Muhsien M.; Salem E. T.; Agool I. R., Preparation and characterization of (Au/n-Sn O2 /Si O2 /Si/Al) MIS device for optoelectronic application, International Journal of Optics, 2013, 756402 (2013) 10.1155/2013/756402

[69] N Naderi and MR Hashim, "Porous-shaped silicon carbide ultraviolet photodetectors on porous silicon substrates," Journal of Alloys and Compounds **552**, 356-362 (2013).

[70] Jurn Y. N.; Malek F.; Mahmood S. A.; Liu W.-W.; Fakhri M. A.; Salih M. H., Modelling and simulation of rectangular bundle of single-walled carbon nanotubes for antenna applications Key Engineering Materials, 701, 57-66 (2016) 10.4028/www.scientific.net/KEM.701.57

[71] Fakhri M. A.; Al-Douri Y.; Hashim U., Fabricated Optical Strip Waveguide of Nanophotonics lthium Niobate, IEEE Photonics Journal, 8(2), 7409919 (2016) 10.1109/JPHOT.2016.2531583

[72] Fakhri M. A.; Salim E. T.; Wahid M. H. A.; Salim Z. T.; Hashim U., A novel parameter effects on optical properties of the LiNbO3 films using sol-gel method, AIP Conference Proceedings, 2213, 20242 (2020) 10.1063/5.0000206